1-2

HIGH ENTHALPY FLOW COMPUTATION AND EXPERIMENT AROUND THE SIMPLE BODIES

A.HANAMITSU T.KISHIMOTO
Kawasaki Heavy Industries, Ltd.

and

H.BITO
National Space Development Agency of Japan

Abstract

High enthalpy shock tunnel test was performed at HEG (High Enthalpy Shock Tunnel in Göttingen) to examine the real gas effect on shock interference heating. Heat transfer distributions were measured along the sphere model and the leading edge of simple wing-body model, whose sweep-back angle on the starboad side is 55° and on the port side is 60° . Flow visualization was also made for simple wing-body model by LIF (Laser Induced Fluorescence) method. CFD analysis has been performed about the heat transfer distribution along the sphere model both in the conditions of frozen flow and equilibrium air flow. Good agreement with experiment was achived in the condition of equilibrium air flow.

This test program was performed under contract with National Space Depelopment Agency of Japan, NASDA, and is a part of wind tunnel test programs for HOPE (H-Ⅱ Orbiting Plane) development.

Introduction

HOPE developement program has been proceeding by NAL and NASDA. Aerothermodynamic design of HOPE is one of the main problem in the design of HOPE config-uration. It is much more severe than that of Space Shuttle Orbiter, because the scale is about one third of Space Shuttle Orbiter. It is required to accurately predict the aerothermodynamic environment during reentry, especially in high temperature hypersonic flight regime, where maximum heat transfer occurs.

To measure heat transfer in high temperature hypersonic flight regime, there are two flight experiment program in Japan. One was the Orbital Reentry Experiment (OREX) project, which was a Japanese first entry experiment from orbit and successfully flied on February 4, 1994. Another is the Hypersonic Flight Experimet(HYFLEX) project, which is planned to be launched by J- Ⅰ Rocket on February, 1996. These flight experimental resuts will give us much information about the aerothermodynamic environ-ment during reentry. But this information is not enough to design HOPE Orbiter. Because OREX and HYFLEX configurations are much different from HOPE; OREX is a capsule type Orbiter and HYFLEX has only fins on the body for lateral stability control, but HOPE is a winged Orbiter with tipfins. This difference means that the problem of local high heating rate caused by the nose bow-shock and leading edge-shock interference still remains. Because the basic configuration of HOPE is a double delta type, a shock interference heating will be an inevitable problem, especially in high temperature hypersonic flight regime, where nose bow-shock is close to the body because of the real gas effect.

To investigate the real gas effect, some high enthalpy shock tunnels were built. But They are not matured yet and they can not simulate completely the real condition. CFD technique, which is not also matured on high enthalpy flows, is required to supplememt the wind tunnel test data.

High enthalpy shock tunnel test was performed at HEG to investigate the real gas effect on heat transfer distribution along the sphere and on shock interference heating for a simple wing-body model, whose sweep-back angle on the starboad side is 55° and on the port side is 60° . The results of the heat transfer measurements are shown and the comparisons of CFD result on heat transfer distribution about the sphere model with experiment are made in this paper.

Test Facility

The HEG(1) is a so called free-piston driven shock tunnel capable of producing high enthalpy and high density test gas flow (figure 1). It is the largest free-piston shock tunnel in the world (60m total length). To create the high pressure of up to 100 MPa in the compression tube, a heavy piston (up to 800 kg and 500 mm in diameter) is used. The nozzle is the hypersonic contoured nozzle. It has an exit diameter of 880 mm, which results in a core flow of about 500 mm.

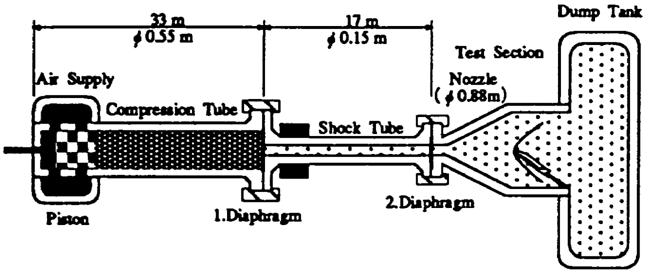

Fig.1 High Enthalpy Shock Tunnel in Göttingen (HEG)

The LIF Method as Applied to HEG

The beams of the two ArF eximer lasers, tuned to different rovibronic transitions of NO, are focused to sheets and introduced to the test section. Since the lasers are fired sequentially in time by some microseconds, the induced fluorescence of each laser is captured only by its corresponding imaging system. These systems consist of an intensified gated CCD-camera combined with a Nikkor uv objective(2).

The plane-convex cylindrical lenses to focus the beams to sheets are mounted in the configuration of a Newton-telescope inside the macrobenches, which also contain the mirrors and beam splitter modules. These modules deflect again only a small percentage of both beams to beam profile CCD-cameras. This enables the recording of each laser sheet before and after its passage through the test section to correct the fluorescence images with respect to laser intensity and profile fluctuations. (Laser intensity and profile change along their path.)

Not only to tune the lasers prior to the wind tunnel run, but also to make quantitative measurement of the detuning (i.e. wavelength drift) for each laser shot during the wind tunnel run, a small percentage of both beams is deflected via the beam splitter module to the heated calibration cell containing NO. An intensified CCD-camera (possibly used with a spectrograph) monitors the induced NO fluorescence of both, spatially separated laser beams.

NO was exicited at around 193 nm. All tests were carried out with three transition lines:

- R_{21}(17.5)
- R_{22}(27.5)
- a mixed line made up of Q_{11}(32.5), Q_{21}(26.5), R_{11}(26.5) and R_{21}(21.5) as the major compoments.

The first two single lines were used to obtain LIF images which could be used for temperature determination, while the last mixed line, which was the strongest line available in the laser tuning range, was used only for flow visualization.

Test Models

The models tested are sphere model and simple wing-body model, which are shown in figure 2. 4 Cu-Ni thin film gages, which were formed on the cylindrical pirex glasses, and 5 chromel-constantan coaxial thermocouples are installed in the sphere model. Cu-Ni thin filem gages were coated with Si02, which makes the surfaces of the gages noncatalytic. Unfortunately they were broken at first shot because of high temperature gas and contamination from the shock tube. (Shock tube inner wall is protected by cupper liner from high stagnation tempature.) Coaxial thermocouples were coverd with epoxy regin for thermal and electrical insulation from the model wall.

The wing-body model has different sweep-back angel to get sweep back angle effect on shock interference heating, 55° on starboad side and 60° on port side. 16 and 18 coaxial thermocouples are installed on the leading edge of the starboad and port side wing, respectively.

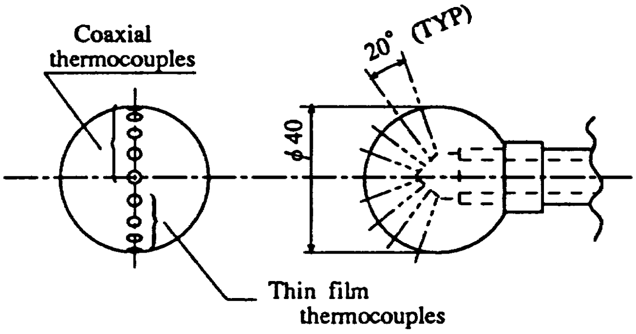

※ Model-sting adapter is provided to rotate the sphere model of ±20°

(a) Sphere Model

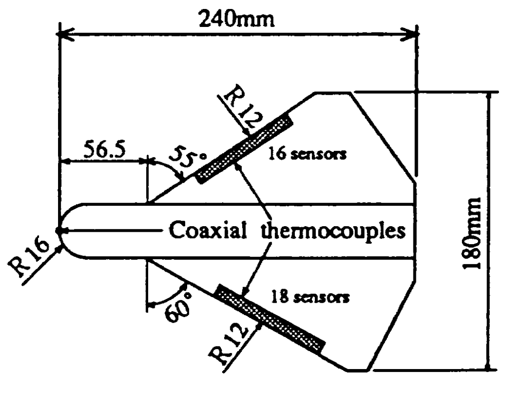

(b) Wing-Body Model

Fig.2 Test Models

Test Conditions

Figure 3 shows three test conditions selected for this test program together with HOPE reentry trajectry and HEG operating envelop. Horizontal axis is total enthalpy and vertical axis is $\rho_\infty L$ termed " binary scal-ing parameter". L is the reference length. Body length (0.24m) was taken as the reference length L in figure 3. These two parameters are very important in high enthalpy flow, because they are similarity parameters for dissociation reactions. Nominal test conditions are also tablated in table 1.

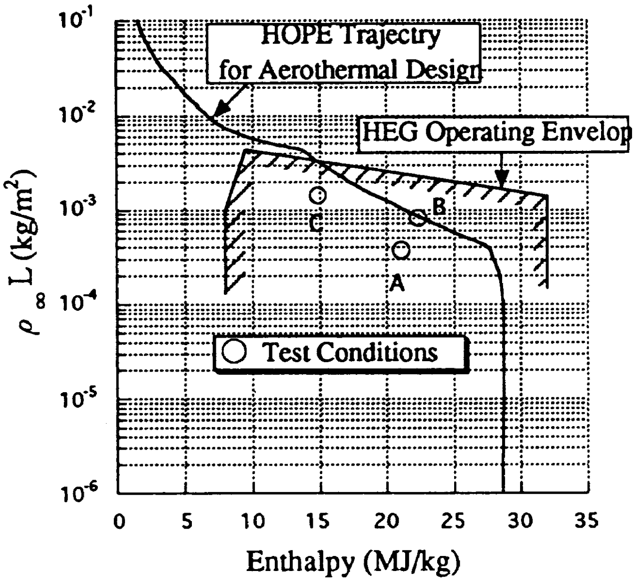

Fig3. Test Conditons and HOPE Reentry Trajectory

Table.1 Nominal Test Conditions

	Conditions		
	A	B	C
Po (MPa)	38.63	90.85	111.1
To (K)	9055	9727	8113
Ho (MJ/kg)	21.06	22.30	14.84
U (m/s)	5939	6180	5151.
$\rho_\infty L$ ($\times 10^{-4}$ kg/m^2)	3.74	8.16	14.09

※ L:Body length=0.24 m

CFD Analysis

Basic equations are Thin-layer Navier-Stokes equations . Flow solver adopted in the present calculations is finite volume TVD upwind scheme⁽³⁾ based on a AUSMDV⁽⁴⁾ scheme Implicit time integration using Gauss Seidel Relaxation method is adopted Computations are performed on the sphere model both in the conditions of frozen gas flow and chemical equilibrium air flow. Curve fitting method⁽⁵,⁶⁾ is used for equilibrium air flow computations.

Grid system is a single domain structured multi-block grid system. Computational grid is shown in figure 4.

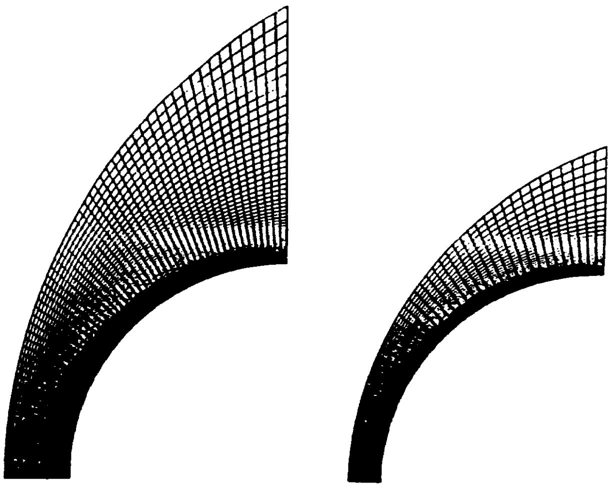

For Perfect Gas Flow (61×81)

For Equilibrium Air Flow (61×81)

Fig.4 Computational Grid for Sphere Model

Heat Transfer Distribution along the Sphere Model

HEG permanent probe (its diameter is 20mm) and sphere model (its diameter is 40mm) were always installed in the test section with other models. Figure 5 shows stagnation point Stanton number vs. Reynolds number based on nose radius. Data from reference (7) are also shown in this figure. Stanton number and Reynolds number were calculated from the flow conditions behind the shock. 1-D nonequilibrium nozzle flow analysis code was used for the computation of free stream conditon and equilibrium code was used for the computation of the condition behind the normal shock.

From this figure, the following relation can be obtained.

$$S_t \propto \left(R_{e,2r}\right)^{-0.5} \propto 1/\sqrt{R_N}$$

This means that the stagntion heat transfer is proportional to square root Reynolds number even in high enthalpy flow condi-tions. Since the stagnation heat transfer is given by

$$\dot{q}_S = S_t R_{e,2r} P_r \cdot \kappa_e (T_{aw} - T_w)$$

However, the level of St is 20~30% higher than estimated data from reference (7), which were taken in the low enthalpy conditons. The cause of this higher level of St may be the catalitic wall effect in HEG conditions. The sensors used were chromel-constantan coaxial thermo-couples, which had metal surfaces, so that the surfaces of the sensors could be considered as fully catalitic wall.

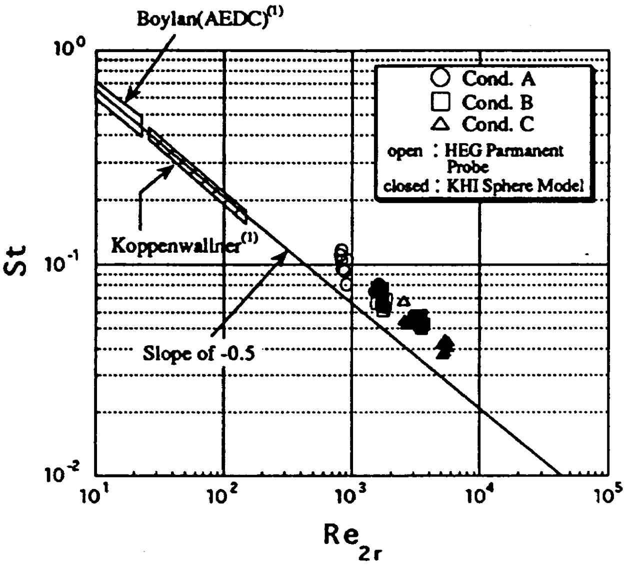

Fig.5 Stagnation Point Stanton Number versus Reynolds Number Based on Nose Radius

Heat transfer distribution along the sphere model in test condition B is shown in figure 6(a). Heat transfer values are normalized by the measured stagnation heat transfer value at θ =0° . The local values vary approximately as con$^{1.5}\theta$, but the value at θ =20° is slightly higher than the stagnation value. Same result was obtained when the sphere model was rotated 20° (see figure 5(b)). In other conditions A and C, same trend was observed. This higher value at θ =20° may be caused by a transition from laminar to turbulent flow, though the Reynolds numbers were too low (see figure 5). It is possible that the sensor can be a trigger of the transision. The sensor was surrounded with epoxy regin, and it slightly melted because of high temperature air and small gap around the sensor was observed. Another possibility is a ununiformity of free stream. (Small disturbance can cause the transition.)

Comparisons of experiments with CFD results were made for three typical test cases of condtion A, B and C. Computations were performed both for the perfect gas (γ =const.) and equilibrium air. The comparison in condition A is shown in figure 7. The result for equi-librium air flow shows good agreement with the experi-ment, but the result for perfect gas flow is about 20% lower in stagnation heat transfer than experiment or equilibrium air result.

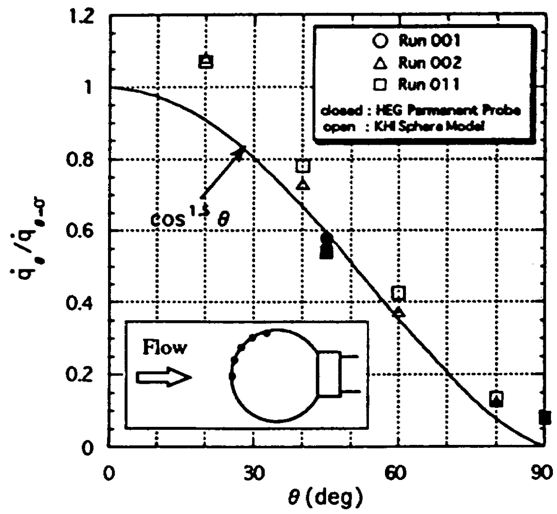

(a) Angle of Attack 0°

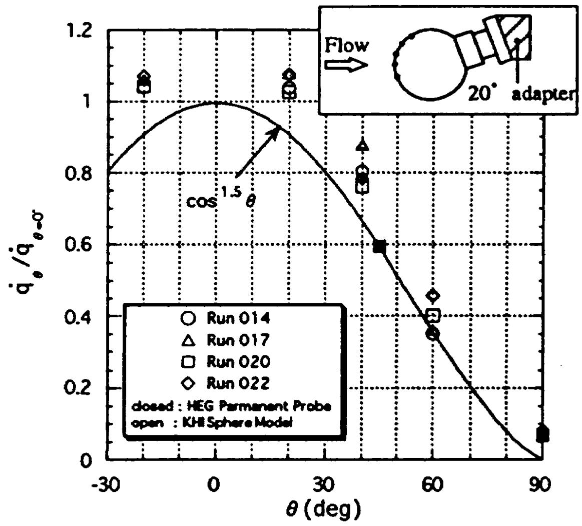

(b) Angle of Attack 20°

Fig.6 Heat Transfer Distribution along the Sphere Model in Condition B

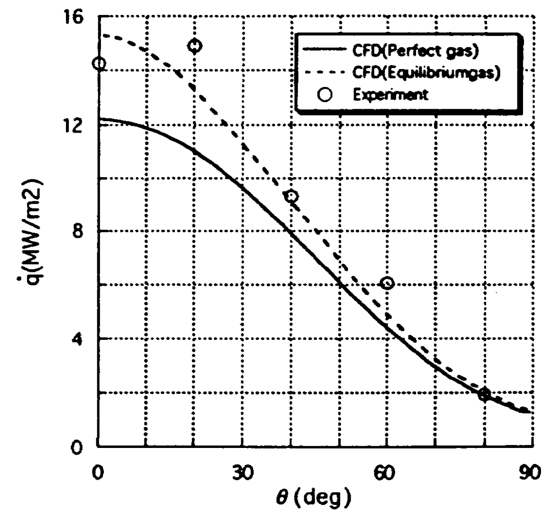

Fig.7 Comparison of Experiment with CFD in Condition A

Heat Transfer Distribution along the Leading Edge of Simple Wing-Body Model

For the delta-wing configuration with highly swept leading edges, the interaction between the bow-generated shock and the wing-generated shock wave exhibit the characteristics of a TYPE VI shock interaction pattern(8). The sketch of the TYPE VI shock interaction pattern is shown in figure 8.

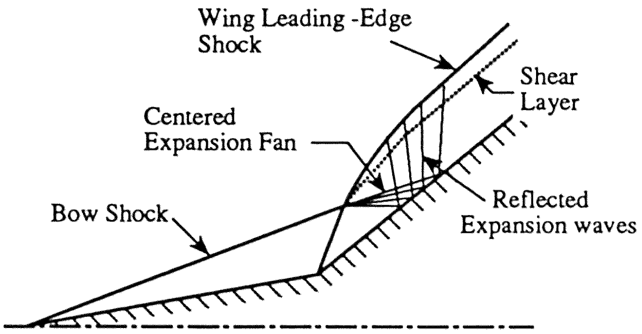

Fig.8 The Sketch of the TYPE VI Shock Interaction Pattern

As has been discussed, the shock interaction for the simple wing-body model will exhibit the characteristics of a TYPE VI shock interaction pattern. Figure 9 is the heat transfer distribution along the leading edge on the starboad side wing; sweep-back angle Λ=55° . In all tests, Angle of attack is 0° . Data are normalized by the nose stagnation heat transfer and η_w is the distance from the wing-root normalized by exposed semi-span.

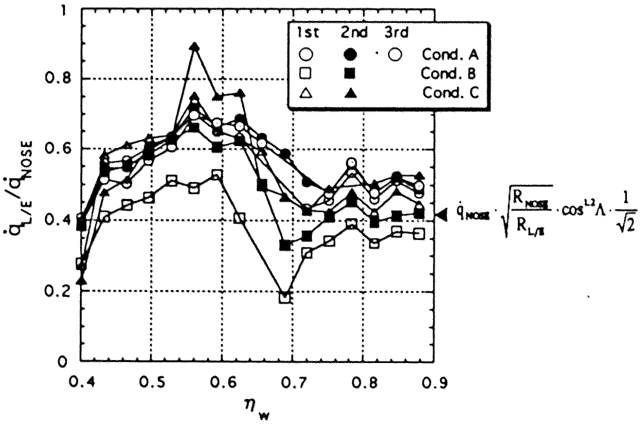

Fig.9 Heat Transfer Distribution Along the Leading Edge with Sweep-Back Angle 55°

Heat transfer near the wing-tip are almost constant so that this region can be considered outside of the shock interference region. The theoretical value without shock interference for oblique cylinder is given by ;

$$\dot{q}_{L/E}=\dot{q}_{NOSE}\cdot\sqrt{\frac{R_{NOSE}}{R_{L/E}}}\cdot\cos^{1.2}\Lambda\cdot\frac{1}{\sqrt{2}}$$

In this equation, sweep-back angle effect is estimated by $\cos^{1.2}\Lambda$, which was derived from the flight data of Space Shattle Orbiter(9). The constant values near the wing-tip agrees well with this theoretical value. But for perfect gas, $\cos^{1.5}\Lambda$ is reported in some papers as the sweep-back angle effect. This means that real gas effect can decrease the sweep-back angle effect on wing leading edge heating.

The LIF images both for Λ=55° and 60° taken at condition B are shown in figure 10. These images show the raw intensity of fluorescence of NO and are not corrected with regard to the laser intensity and profile fluctuations. But the colors of the LIF image are almost proportional to the temperature and density of NO molecule. The shock impingement point on the wing of Λ=55° could be read to about η_w=0.6 from this figure. The maximum heating occurs just inside this point, and is about 1.5 times as large as the values without shock interference.

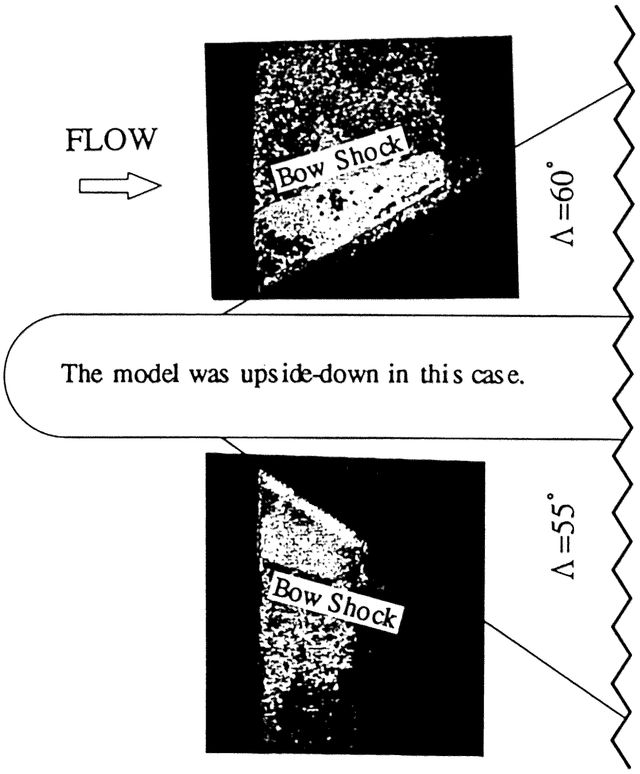

Fig.10 LIF images in Condition C

For a basic TYPE VI shock interaction pattern, the heating increases uniformly in the portion of the leading edge subjected to the flow within the bow shock and there are no localized increases in heating(10). However a localized increase can be seen clearly in figure 9. One of this reason may be like this; the bow shock is generated by the spherical nose so that the total pressure within the bow shock along each stream line is different, i.e. the total pressure loss along the stream line which pass though the bow shock near the nose is larger than that pass though pressure loss along the stream line which pass though the bow shock near the nose is larger than that pass though the oblique bow shock.. These gives the nonuniform heating within the bow shock.

The higher heat transfer within the bow shock than that without shock interference is partly caused by the difference of the flow properties between inside and outside of the bow shock. The flow coming to the portion of the leading edge within the bow shock passes through two weak oblique shock waves; the bow shock and leading edge shock. On the other hand, the flow coming to the portion of the leading edge outside of the bow shock passes through only one shock wave; the leading edge shock. The total pressure loss of the former flow is lower than that of the latter flow. However, the the flow direction is deflected through the bow shock, which results in the increase of the effective sweep-back angle of the leading edge with respect to the flow. This cancels some part of the increase in heating caused by the smaller total pressure loss. Further investigations should be made to understand the reasons for the increase in heating within the bow shock.

Figure 11 shows the heat transfer distribution for $\Lambda=60^\circ$. From figure 10, shock impingement point is about $\eta_W=0.7$. Heat transfer data are very scattered, but trend and the ratio of maximum heat transfer to outer wing value are almost same as that for $\Lambda=55^\circ$. The heat transfer distribution within the bow shock is relatively uniform for $\Lambda=60^\circ$, which will be cuased by the difference of the sweep-back angle effect. Sweep-back angle effect for $\Lambda=60^\circ$ is larger than that for $\Lambda=55^\circ$ so that the heat transfer distribution within the bow shock will be smoothed.

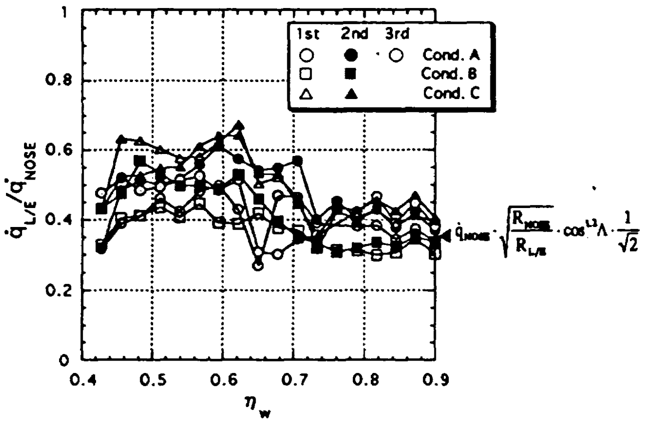

Fig.11 Heat Transfer Distribution Along the Leading Edge with Sweep-Back Angle 60°

The decrease in heating caused by the expansion fan generated from the intersection of the bow shock and wing shock can be seen just outside of the bow shock in some cases for $\Lambda=55^\circ$. But there are no distinct decrease in heating for $\Lambda=60^\circ$. It is possible that three-dimesional effect, i.e. cross flow, is dominant near the leading edge so that the influence of the expansion fan can not be seen as clear as in the two-dimensional case.

Conclusions

High enthalpy shock tunnel test was performed at HEG under contract with NASDA for sphere model and simple wing-body model. Comparison of measured heat transfer distribution along the sphere model with CFD both for the perfect gas flow and equilibrium air flow has been made. Based on the experimental result and present computations, the following conclusions are made.

1) The slope of the stagnation Stanton number with regard to the stagnation Reynolds number showed good agreement between high and low enthalpy flow. However, Stagnation heat transfer of the spherical nose in high enthalpy flow showed a 20～30% higher value than that in low enthalpy flow (perfect gas flow).
2) Measured heat transfer at $\theta=20^\circ$ of the sphere model showed the higher value than the stagnation value in all test conditons. CFD analysis for laminar flow didn't give such a result so that this would be caused by a transition from laminar to turbulent flow.
3) Good agreement of CFD results for an equilibrium air flow with experiment in heat transfer distribution along the sphere has been obtained. But perfect gas computations gave the lower value than the values for an equilibrium air flow or experiment. This is consistent with the statement 1).
4) Though the shock interference pattern for the simple wing-body model had been considered as a TYPE VI and there would be no localized increase in heating, a localized peak heating just inside the bow shock was observed in this experiment. This will be cuased that the degree of the total pressure loss of the flow within the bow shock varies along the leading edge.
5) The maximum heating on the leading edge of the simple wing-body model occured just inside the bow shock,which value is about 1.5 times as large as the value without the shock interference. The heat transfer outside of the shock interference region agrees well with the theoretical value.

References

(1)G.Eitelberg, T.J.McIntyre, and W.H.Beck, "The High Enthalpy Shock Tunnel in Göttingen," AIAA 92-3942, 1992.

(2)W.H.Beck, C.Dankert, G.Eitelberg, and G.Gundlach, "Preliminary Laser Induced Fluorescence Measurements in Several Facilities in Preparation for Application to Studies in the High Enthalpy Shock Tunnel Gottingen (HEG)," AIAA 92-0143, 1992.

(3)Sawada,K., and Takanashi,S., "A Numerical Investigation on Wing/Nacelle Interferences of USB Configuration," AIAA 87-0455, 1987.

(4)Wada,Y., and Liou,M., "A Flux Splitting Scheme with High-Resolution and Rubustness for Discontinuities," AIAA 94-0083, 1994.

(5)Srinivasan,S., Tannehill,J.C., and Weilmuenster,K. J., "Simplified Curve Fits for the Thermodynamic Properties of Equilibrium Air," ISU-ERI-Ames-86401, ERI Project 1626, CFD 15, 1986.

(6)Srinivasan,S., and Tannehill,J.C., "Simplified Curve Fits for the Transport Properties of Equilibrium Air," NASA-CR-178411, 1987.

(7)J.D.Anderson, Jr., "Hypersonic and High Temperature Gas Dynamics," McGraw-Hill Series in Aeronautical and Aerospace Engineering, 1989, p.257, quoted from Koppenwallner,G., "Fundamentals of Hypersonics :Aerodynamics and Heat Transfer," in the Short Course Notes entitled Hypersonic Aerothermodynamics, presented at the von Karman Institute for Fluid Dynamics, Rhose Saint Genese, Belgium, 1984.

(8)J.J.Bertin, S.J.Mosso, and D.W.Barnette, " Engineering Flowfields and Heating Rates for Highly Swept Leading Edges," Journal of Spacecraft and Rockets, Vol.13, No.9, 1976, pp.540-546.

(9)J.A.Cunningham, and J.W.Haney, Jr., "Space Shuttle Wing Leading Edge Heating Environment Prediction Derived from Development Flight Data", NASA -CP-2283 Part II, " Shuttle Performance: Lessons Learned", 1983.

(10)J.J.Bertin, and B.W.Graumann, "Hypersonic Shock-Interaction Phenomina Applicable to Space Shuttle Configurations," NASA-CR-128586, 1972.